Impact of biaxial and uniaxial strain on V_2O_3

Darshana Wickramaratne [1] Noam Bernstein,[2] and I. I. Mazin [2,*]

[1]*NRC Research Associate, Resident at Center for Computational Materials Science, U.S. Naval Research Laboratory, Washington, DC 20375, USA*

[2]*Center for Computational Materials Science, U.S. Naval Research Laboratory, Washington, DC 20375, USA*

Using first-principles calculations, we determine the role of compressive and tensile uniaxial and equibiaxial strain on the structural, electronic, and magnetic properties of V_2O_3. We find that compressive strain increases the energy to transition from the high-temperature paramagnetic metallic phase to the low-temperature antiferromagnetic insulating phase. This shift in the energy difference can be explained by changes in the V-V bond lengths that are antiferromagnetically aligned in the low-temperature structure. The insights that we have obtained provide a microscopic explanation for the shifts in the metal-insulator transition temperature that have been observed in experiments of V_2O_3 films grown on different substrates.

I. INTRODUCTION

The metal-to-insulator transition (MIT) in V_2O_3 [1] has been the subject of intense investigations, due in part to the coupled structural, electronic, and magnetic phase transitions that occur in the material [2,3]. Above the bulk MIT temperature T_c of 155 K, V_2O_3 is a metal and is stable in the corundum phase. Below T_c, V_2O_3 undergoes a structural transition from corundum to monoclinic. This is accompanied by the opening of a Mott gap of 0.40 eV below the MIT T_c, which manifests in a large increase in the electrical resistivity [4]. The co-occurrence of these phenomena has led to several efforts that have sought to control these phase transitions.

To understand and control the MIT in V_2O_3 it is important to consider the underlying microscopic mechanism that leads to the transition. While it is well accepted that above T_c the electronic phase is metallic and below T_c it is a Mott insulator, the mechanism leading to the MIT cannot be described as a Mott transition. It is only recently, through a combination of neutron scattering measurements and first-principles calculations, that Leiner *et al.* convincingly demonstrated that it is instead a first-order phase transition between two states that host different magnetically ordered states in addition to being structurally and electronically distinct above and below the MIT T_c [3]. The metallic high-temperature (HT) phase was shown to be a strongly frustrated paramagnet, and the insulating low-temperature (LT) phase is a robust antiferromagnet with little frustration. Since the structural, electronic, and magnetic properties of V_2O_3 are intimately linked, this makes the metal-insulator transition temperature sensitive to external perturbations.

Indeed, we have shown that the presence of point defects in the form of Frenkel pairs disrupts bonding and the magnetic ordering of the V atoms, which in turn leads to a reduction in

the energy to transition between the HT paramagnetic metallic phase and the LT antiferromagnetic insulating phase [5]. This is consistent with an experimental observation that found the MIT T_c to decrease when point defects are introduced intentionally compared to the T_c of as-grown V_2O_3 [6]. The sensitivity of the MIT to changes in bonding has also made the use of strain an appealing approach to manipulate and control the MIT. This is part of a general growing interest in manipulating the transition temperature of materials that exhibit a MIT by taking advantage of advances in epitaxial growth, which has enabled the growth of thin films on targeted substrates [7].

Epitaxial growth of V_2O_3 on a-plane ($11\bar{2}0$), c-plane (0001), m-plane ($1\bar{1}00$), and r-plane ($1\bar{1}02$) Al_2O_3 substrates has been explored by a number of groups [8–14]. Growth of V_2O_3 on these substrates occurs at a temperature well above the MIT T_c, which results in a film that presumably adopts the HT paramagnetic corundum structure during growth. The Al_2O_3 lattice constants are lower than the corundum V_2O_3 lattice constants, so V_2O_3 is expected to be under compressive strain if the growth is coherent. The reports of T_c identified from measurements of resistance versus temperature of these epitaxially grown films are varied. Schuler *et al.* demonstrated that the T_c increases by 45 K with respect to unstrained V_2O_3 in a cooling cycle measurement of resistance versus temperature for V_2O_3 grown on c-plane Al_2O_3 [13]. In contrast, Kalcheim *et al.* [10] demonstrated that V_2O_3 grown on the m-plane and r-plane orientations of Al_2O_3 led to a T_c that is larger than the unstrained T_c (by up to 16 K), while growth on the a-plane orientation of Al_2O_3 led to a reduction in T_c. Growth on alternative substrates, such as $LiTaO_3$, has also been explored where V_2O_3 is expected to be under tensile strain if the growth is coherent [9,15,16]. In these studies, it was found that the T_c of V_2O_3 was larger than the T_c of unstrained V_2O_3. An alternative approach to impart strain on V_2O_3 has been through the use of ferroelectric and piezoelectric substrates that are subject to electrical biases with different polarity [17,18]. For instance, the T_c of V_2O_3

---

*Present address: Department of Physics and Astronomy, George Mason University, Fairfax, VA 22030, USA.

on a PMN-PT substrate increased by 30 K when the PMN-PT substrate underwent tensile expansion due to an applied bias.

The results of these experimental studies have been interpreted using the pressure versus temperature phase diagram of V_2O_3 [1]. According to this phase diagram, positive pressure (volume reduction) leads to a reduction in T_c while negative pressure (volume expansion) leads to an increase in T_c. However, for a material under uniaxial or biaxial strain, the corresponding change in bonding can be very different from the change in bonding associated with hydrostatic pressure. Furthermore, first-principles calculations have demonstrated that relying on chemical pressure alone to interpret the V_2O_3 phase diagram can be misleading [19]. To our knowledge, the impact of strain on the structural, magnetic, and electronic properties of V_2O_3 has not yet been theoretically studied. Because of this, there is no clear relationship that can be deduced from the experimental reports on changes in the V_2O_3 T_c grown on different substrates and the magnitude and direction of the strain imparted.

In this study, we use first-principles calculations to investigate the effect of uniaxial and equibiaxial compressive and tensile strains on the structural, magnetic, and electronic properties of V_2O_3. We find that up to 1% compressive equibiaxial or uniaxial strains increase the energy required to transition to the LT antiferromagnetic insulating phase by up to 75% compared to unstrained V_2O_3. This would be reflected in an increase in the MIT T_c when V_2O_3 is under compressive strain. In contrast, we find equibiaxial tensile or uniaxial tensile strains lead to modest reductions or increases in the energy to transition to the antiferromagnetic insulating phase depending on the direction along which the strain is imparted. We identify the microscopic origin of these changes in the energy to transition between the metallic and insulating phase as being changes in the bond lengths of the pair of next-nearest-neighbor vanadium atoms that are antiferromagnetically aligned in the LT monoclinic structure.

II. COMPUTATIONAL METHODS

Our calculations are based on density functional theory within the projector-augmented wave method [20] as implemented in the VASP code [21,22] using the generalized gradient approximation defined by the Perdew-Burke-Ernzerhof (PBE) functional [23]. In our calculations, V $4s^2 3p^6 3d^3$ electrons and O $2s^2 2p^4$ electrons are treated as valence. All calculations use a plane-wave energy cutoff of 600 eV. Structural relaxations of the lattice parameters and internal coordinates were carried out with an $8 \times 8 \times 8$ k-point grid and a force convergence criterion of 5 meV/Å. To simulate the Mott-insulating behavior of V_2O_3, we use a spherically averaged Hubbard correction within the fully localized limit double-counting subtraction [24]. We apply a U-J value of 1.8 eV to the V d-states, which reproduces the experimental band gap of V_2O_3. We note studies that compared exchange-coupling constants obtained from neutron scattering with first-principles calculations that relied on a larger value of U-J (3 eV) to obtain quantitative agreement between theory and experiment [3]. We find our overall conclusions to remain unchanged if we also use a U-J value of 3 eV.

To study the effects of epitaxial strain, we performed "strained-bulk" calculations where we impose compressive and tensile equibiaxial strain on the a and b (denoted as ab), b and c (denoted as bc), and a and c (denoted as ac) monoclinic lattice vectors, and uniaxial strain along the a, b, and c monoclinic lattice vectors of the V_2O_3 unit cell, and then we optimize the free lattice constant(s) and all atomic positions of the unit cell. The standard VASP package does not allow for arbitrary constraints to be placed on the strain tensor during relaxation. To perform these constrained calculations, we made modifications that set specific components of the stress tensor to zero during the minimization routine. This allowed us to impose strain along the different axes as we report here.

Since growth of V_2O_3 occurs at temperatures well above the MIT T_c, the as-deposited V_2O_3 epitaxial films will adopt the HT paramagnetic structure. Paramagnetically ordered states are challenging to describe with standard DFT. However, since the paramagnetic HT phase is magnetically frustrated [3], magnetic ordering has a weak effect on total energies. We have previously shown that the FM ordered monoclinic structure can be used as a suitable proxy for the paramagnetic HT corundum phase [5]. Since strain is defined with respect to the HT phase, we use the lattice constants of the HT ferromagnetic structure as the reference for strain. For example, uniaxial strain along the monoclinic a axis, ϵ_a, is defined as $\epsilon_a = [(a - a_0)/a_0]$, where a_0 is the equilibrium a lattice constant of the FM monoclinic structure. In such a calculation, we would only allow the monoclinic b and c lattice constants, bond angles, and atomic coordinates to be optimized. Next, with this optimized structure we impose an AFM ordering of spins on the V atoms (ferromagnetic along the a and c axes and antiferromagnetic along the b axis), and we optimize the free lattice parameters and atomic coordinates. We report results for compressive and tensile strain along each of the monoclinic axes for strains that range between $\pm 1\%$. Positive values of ϵ correspond to tensile strain.

III. RESULTS

A. Bulk properties

The HT metallic phase of V_2O_3 is stable in the corundum structure with space group $R\bar{3}c$. Neutron scattering measurements in combination with first-principles calculations have demonstrated the corundum phase of V_2O_3 to be a highly frustrated paramagnet [3]. As we discuss in Sec. II, we use a FM ordered structure as a proxy for the disordered paramagnetic phase of the corundum HT structure since it has the correct magnitude of the magnetic moments and it respects the full lattice symmetry (as opposed to an antiferromagnetic arrangement of spins). Indeed, we have previously shown that the energy difference between the corundum structure with FM order and AFM order imposed is low, 0.8 meV per vanadium atom [5], consistent with the magnetic frustration that has been experimentally identified in the HT phase [3]. Our DFT $+ U$ lattice constants of the FM corundum structure are $a = b = 5.037$ Å and $c = 14.305$ Å, and the bond angle of the rhombohedral unit cell is $\theta = 54.6°$, which are within
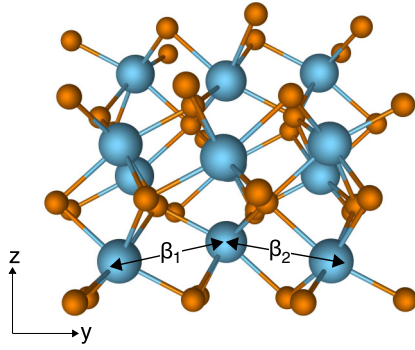
FIG. 1. Schematic illustration of the V_2O_3 monoclinic unit cell. Vanadium atoms are in blue and oxygen atoms are in orange. The pair of V atoms that are antiferromagnetically aligned along the monoclinic b axis are denoted β_1 and β_2.

1.5% of the experimentally measured lattice parameters of the HT corundum structure ($a = b = 4.952$ Å, $c = 14.003$ Å, and $\theta = 56.1°$).

The LT insulating phase of V_2O_3 is antiferromagnetic and has a monoclinic structure with space group $P2_1/c$. We find the lattice constants of the LT monoclinic structure of V_2O_3 to be $a = 7.414$ Å, $b = 5.084$ Å, and $c = 5.559$ Å, and the bond angles to be $\alpha = \gamma = 90°$ and $\beta = 97.3°$, which are within 2.7% of the experimental LT lattice parameters ($a = 7.255$ Å, $b = 5.002$ Å, $c = 5.548$ Å, and $\beta = 96.8°$) reported for monoclinic V_2O_3 [25]. To describe the antiferromagnetic ordering of spins, we use a four-formula-unit cell. We find the ground-state magnetic ordering to be the one where the V atoms are aligned ferromagnetically along the monoclinic a and c axes and aligned antiferromagnetically along the monoclinic b axis, which is consistent with neutron scattering measurements of the monoclinic insulating phase [3,26].

Along the monoclinic b-axis, the pair of next-nearest-neighbor V atoms that are antiferromagnetically aligned have two different V-V bond lengths. We label the shorter of the two bonds β_1, and the second V-V pair is labeled β_2, as shown in Fig. 1. The bond length of the β_1 pair is 2.996 Å, while the bond length of the β_2 pair is 3.085 Å.

Since we are interested in the impact of strain on the energy to transition between the paramagnetic (approximated as ferromagnetic) HT phase and the antiferromagnetic LT phase using the "strained-bulk" approach, we also calculate the lattice parameters and electronic properties of the monoclinic structure where all of the V atoms are ferromagnetically aligned. If we allow for full structural relaxation (volume, cell shape, and atomic positions) in this magnetic state, we find that the structure takes on the HT corundum structure and is metallic.

B. Biaxial and uniaxial strain

1. Structural properties

For the magnitudes of strain that we have investigated, we find that biaxial and uniaxial strain leads to elastic changes in the volume and in turn in the free lattice parameter(s). The monoclinic bond angle only changes by up to $\pm 0.2\%$ for the largest strain ($\pm 1\%$) that we consider.

If we consider biaxial strain imposed along the monoclinic ab axes, applying compressive equibiaxial strain to the FM structure and allowing the monoclinic c lattice parameter and all atomic positions to relax leads to an increase in the c lattice constant. We find that the c lattice constant increases linearly as a function of the applied compressive strain. Conversely, for equibiaxial tensile strain, the c lattice constant decreases linearly with respect to the c lattice constant of the unstrained FM structure. The ratio of the change in the c lattice constant as a function of the applied equibiaxial in-plane strain is a positive constant in the elastic regime and is defined as the Poisson ratio, $\nu = -\epsilon_{zz}/(\epsilon_{xx} + \epsilon_{yy})$, where ϵ_{zz} is the strain in the c lattice constant, and ϵ_{xx} and ϵ_{yy} are the strains along the a and b monoclinic lattice constants, respectively. We find $\nu = 0.31$ for the FM structure under equibiaxial strain along the ab axes. We find the response of the V_2O_3 lattice to equibiaxial strain along the bc and ac axes to be similar; the free lattice parameter changes linearly with a Poisson ratio that is positive. $\nu = 0.33$ for the FM structure under equibiaxial strain along bc, and $\nu = 0.32$ for equibiaxial strain along ac.

Next we impose AFM ordering on the structures that are under equibiaxial or uniaxial tensile strain. As discussed in Sec. II, we assume that the lattice parameters of the HT paramagnetic (approximated as FM) would be clamped to the substrate post-growth and these lattice parameters remain fixed when the transition to the LT AFM insulating phase occurs. For example, for equibiaxial strain along the monoclinic ab axis, ϵ_{ab}, of 1% (where ϵ_{ab} is with respect to the equilibrium FM lattice parameters), we use the same monoclinic a and b lattice parameters that are strained by 1% with respect to the equilibrium FM monoclinic lattice constants, we impose AFM order, and we allow the monoclinic c lattice constant and all atomic coordinates to relax.

For each of the structures under strain with AFM order imposed, we find that the lattice also responds elastically with a positive Poisson ratio. The magnitude of ν for the structures that are antiferromagnetically ordered for the different directions of equibiaxial strain are as follows: $\nu = 0.36$ (ab), 0.38 (bc), and 0.33 (ac).

2. Total energies

In Fig. 2, we illustrate the variation in the total energy of the FM and AFM configuration under biaxial strain along the monoclinic ab and bc axes and uniaxial strain along the monoclinic b axis. It is evident that the AFM configuration remains lower in energy than the FM configuration for all values of strain. For each of these values of strain, the FM configuration remains metallic while the AFM configuration remains insulating.

3. Spin-flip energies

From Fig. 2 it is also evident that the energy to transition between the high-temperature FM configuration and the low-temperature AFM configuration as a function of compressive and tensile strain is not a constant. For example, the total energy difference between the AFM and FM configuration under biaxial strain along ab is larger under compressive strain compared to tensile strain. We define this energy difference
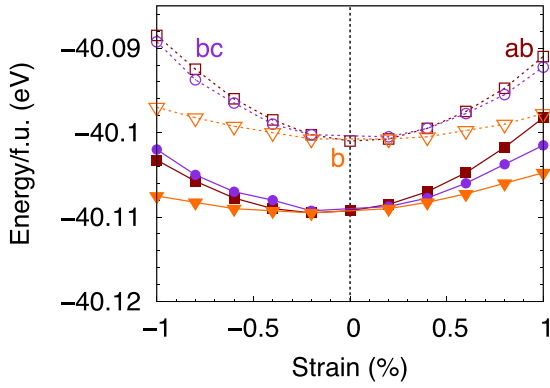
FIG. 2. Variation in the total energy of the AFM (solid line) and FM (dotted line) configuration per V_2O_3 formula unit under compressive and tensile strain along the monoclinic ab (□), bc (○), and b (▽) axes. The vertical black dotted line denotes zero strain. Note, strain is defined with respect to the equilibrium lattice constants of the FM structure.

between the AFM and FM configuration at a fixed strain, ϵ, a spin-flip energy, ΔE, where $\Delta E = [E_{tot}(AFM) - E_{tot}(FM)]$. Note that since the AFM configuration remains lower in energy than the FM configuration for all values ($\pm 1\%$) and directions of strain that we consider in this study, ΔE is always negative. An increase in the magnitude of ΔE corresponds to an increase in the energy required to transition from the insulating AFM to the metallic paramagnetic (approximated as FM) state, while a reduction in the magnitude of ΔE corresponds to a reduction in the energy to transition from the AFM to the FM state. The spin-flip energy as a function of equibiaxial and tensile strain is illustrated in Fig. 3.

We first consider the change in spin-flip energy for the structures subject to equibiaxial strain. Under compressive strain along the ab and bc axes, the magnitude of ΔE, which is the energy required to transition from the insulating AFM state to the metallic FM state, increases by up to 75% at the largest value of ϵ of 1%. Tensile strain along these axes
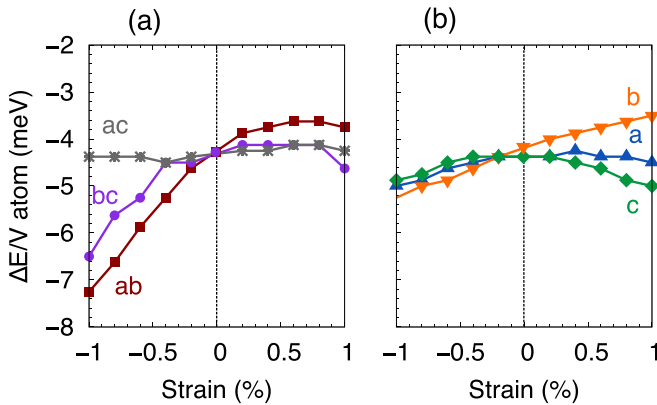

FIG. 3. Spin-flip energy, $\Delta E = [E_{tot}(AFM) - E_{tot}(FM)]$, per V atom as a function of compressive and tensile (a) biaxial strain along the monoclinic ab (□), bc (○), and ac (∗) axes, and (b) uniaxial strain along the monoclinic a (△), b (▽), and c (◇) axes. The vertical black dotted line denotes zero strain. Note, strain is defined with respect to the equilibrium lattice constants of the FM structure.

leads to a modest reduction in the magnitude of ΔE for strain along ab and a modest increase in the magnitude of ΔE for ϵ greater than 0.5% along bc. In contrast, we find that ΔE is insensitive to compressive and tensile equibiaxial strain along the monoclinic ac axes.

When V_2O_3 is subject to uniaxial strain, we find the change in ΔE to be modest in comparison to the change in ΔE under biaxial strain. In particular, when the monoclinic a, b, or c axes are under compressive strain, we find they all lead to a slight increase in the magnitude of ΔE. Under tensile uniaxial strain, the magnitude of ΔE increases for strain along the a and c axes, while the magnitude of ΔE decreases for tensile strain along the b axis.

IV. DISCUSSION

At this point, it is instructive to examine the primary contributions to the change in ΔE under compressive and tensile strain. We decompose this change in ΔE into two contributions, namely an elastic energy, ΔE^{el}, and a magnetic energy, ΔE^{mag}, such that $\Delta E = \Delta E^{el} + \Delta E^{mag}$. The elastic energy, ΔE^{el}, is the change in energy due to the change in the lattice parameters and the atomic positions to transition from the geometry associated with the FM to the AFM configuration at a fixed magnetic configuration. We define ΔE^{el} as $[E_{tot}^{[\epsilon,FM]}(AFM) - E_{tot}^{[\epsilon,AFM]}(AFM)]$, where $E_{tot}^{[\epsilon,FM]}(AFM)$ is the total energy of the structure with the atomic coordinates and lattice parameters of V_2O_3 in the strained FM configuration with AFM order imposed, and $E_{tot}^{[\epsilon,AFM]}(AFM)$ is the total energy of the structure with the atomic coordinates and the lattice parameters in the strained AFM configuration and AFM order imposed. The magnetic energy, ΔE^{mag}, is the change in energy associated with flipping spins from ferromagnetic to antiferromagnetic at a fixed set of atomic coordinates and lattice parameters. We define ΔE^{mag} as $[E_{tot}^{[\epsilon,AFM]}(AFM) - E_{tot}^{[\epsilon,AFM]}(FM)]$, where $E_{tot}^{[\epsilon,AFM]}(AFM)$ is the total energy of the structure with the atomic coordinates and lattice parameters of the strained AFM configuration with AFM order imposed, and $E_{tot}^{[\epsilon,AFM]}(FM)$ is the total energy of the structure with the atomic coordinates and lattice parameters of the strained AFM configuration with FM order imposed. For all values of biaxial and uniaxial strain, ΔE^{el} only changes by up to 0.5 meV per vanadium atom. Note, ΔE changes by up to ~4 meV per vanadium atom in comparison to unstrained V_2O_3 (Fig. 3). Hence, the remaining energy difference between ΔE and ΔE^{el} is the change in the magnetic energy, ΔE^{mag}, as a function of strain.

Based on Fig. 3, it is evident that ΔE is more sensitive to compressive strain in V_2O_3. To explain this sensitivity to compressive strain, we examine the bond lengths of V_2O_3 in the AFM configuration. In the AFM configuration, the V atoms are ferromagnetically coordinated along the a and c axes and antiferromagnetically coordinated along the b axis. Previous first-principles calculations of the unstrained V_2O_3 lattice [3] have demonstrated that the V atoms along the monoclinic b axis have the largest exchange coupling constants compared to the next-nearest-neighbor V-V exchange coupling constants along the other axes of the monoclinic structure. Within a nearest-neighbor Heisenberg model, the Néel temperature of the HT paramagnetic to the LT AFM phase transition would
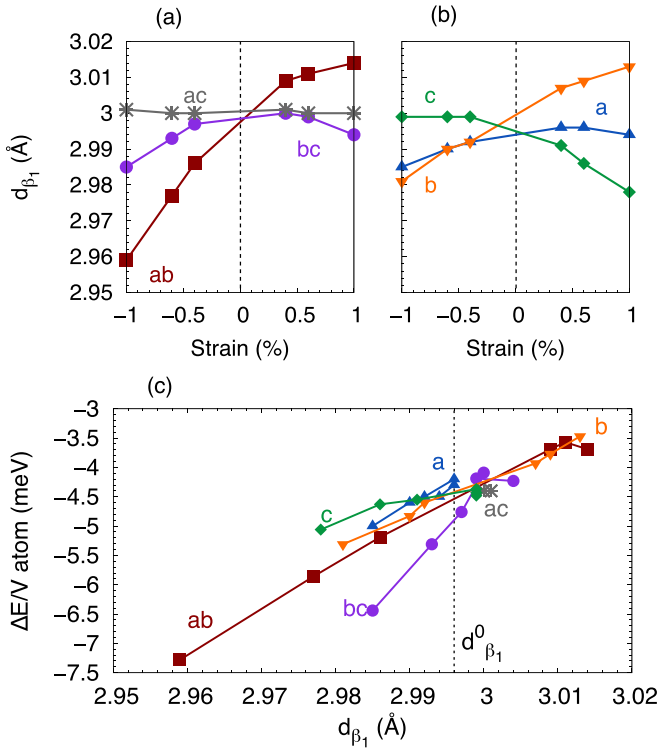
FIG. 4. Change in the bond length, d_{β_1} (cf. β_1 in Fig. 1), as a function of compressive and tensile (a) biaxial strain along the monoclinic ab ($\square$), bc ($\circ$), and ac ($\ast$) axes, and (b) uniaxial strain along the monoclinic a ($\triangle$), b ($\triangledown$), and c ($\diamond$) axes. The vertical black dotted line denotes zero strain. Note, strain is defined with respect to the equilibrium lattice constants of the FM structure. (c) Spin-flip energy vs change in the d_{β_1} bond length for the different directions of compressive and tensile strain imparted on the monoclinic axes. The d_{β_1} bond length of unstrained AFM V_2O_3 ($d_{\beta_1}^0 = 2.996$ Å) is shown with a dotted black line.

be determined primarily by the exchange coupling constants of these antiferromagnetically aligned V atoms. We denote these V-V bonds along the monoclinic b axis as β_1 and β_2 (Fig. 1), where the bond length of β_1 (d_{β_1}) is shorter than the bond length of β_2 (d_{β_2}). Leiner et $al.$ [3] have shown that the exchange coupling constant of β_1 is twice as large as that of β_2.

Through our first-principles calculations, we find that d_{β_1} changes nonmonotonically as a function of compressive and tensile strain. These results are illustrated in Figs. 4(a) and 4(b). Figure 4(c) illustrates the dependence of ΔE on d_{β_1} for the different directions of strain we consider in our study. When d_{β_1} decreases with respect to d_{β_1} of the unstrained AFM monoclinic structure, we find that the magnitude of ΔE, which is the energy to transition from the insulating AFM to the metallic FM state, increases, while an increase in d_{β_1} corresponds to a reduction in the magnitude of ΔE. Since the primary contribution to the change in ΔE is the magnetic energy, this dependence of ΔE on d_{β_1} can be understood as follows. A reduction in the d_{β_1} bond length is expected to lead to an increase in the hopping energy, t, between the β_1 pair of vanadium atoms (Fig. 1), which in turn would lead to an increase in the exchange coupling constant, J_{β_1},

where $J_{\beta_1} \propto -t^2/U$, and U is the on-site Coulomb repulsion. Conversely, we expect an increase in d_{β_1} to lead to a reduction in J_{β_1} compared to unstrained V_2O_3. This dependence of ΔE on d_{β_1} also explains why equibiaxial compressive and tensile strain along the monoclinic ac axes does not lead to a change in ΔE. We find that the biaxial strain that is imparted on the ac axes is accommodated by changes in d_{β_2} while d_{β_1} remains unchanged for all values of strain that we investigate [Fig. 4(a)].

Hence, our calculations suggest that the MIT T_c is sensitive to changes in the bond length, d_{β_1}. In particular, we suggest that compressive strain along the monoclinic bc, ab, a, b, and c axes and tensile strain along the monoclinic bc, a, and c axes will increase T_c compared to unstrained V_2O_3. We note that this is consistent with the increase in the MIT T_c that has been measured in V_2O_3 thin films grown on Al_2O_3 substrates, where V_2O_3 is under compressive strain [8–10,13].

V. SUMMARY AND CONCLUSIONS

In summary, we examined the role of equibiaxial and uniaxial compressive and tensile strain on the electronic, structural, and magnetic properties of V_2O_3.

The metal-insulator transition in V_2O_3 was recently reinterpreted as being a strong first-order transition between the high-temperature corundum structure, which is a highly frustrated paramagnet, and the low-temperature monoclinic structure, which is strongly antiferromagnetic [3]. The leading contribution to the strong antiferromagnetic coupling in the low-temperature monoclinic phase is the shortest of the pair of V-V bonds that are antiferromagnetically aligned (β_1) along the monoclinic b axis. As a result, shifts in the energy difference between the high-temperature metallic phase and the low-temperature insulating phase are sensitive to changes in the bond length of β_1 of the LT AFM monoclinic phase. Our calculations confirm this interpretation and demonstrate that changes in the bond length of β_1 due to strain can lead to changes in this energy difference. In particular, we find that a suppression of this energy difference, which would translate to a reduction in the MIT T_c, coincides with an elongation of the bond length of β_1 while an increase of this energy difference coincides with a compression of the β_1 bond length.

Based on our calculations, we can draw the following conclusions on the role of strain on the metal-insulator transition temperature of V_2O_3. Under compressive strain along the monoclinic bc, ab, b, a, and c axes, the energy to transition to the low-temperature insulating antiferromagnetic phases increases by up to 75% for compressive strains up to 1%. Tensile strain along the monoclinic a and c axes leads to modest increases in the energy to transition to the insulating antiferromagnetic phase. Hence, strain along these directions and axes will likely lead to an increase in T_c compared to unstrained V_2O_3. Tensile strain along the ab and b axes lowers the energy to transition to the insulating phase by up to 10% compared to unstrained V_2O_3 for the largest strain we consider of 1%, which would be reflected in a reduction in T_c compared to unstrained V_2O_3. In contrast, compressive and tensile strain along the monoclinic ac axes does not lead to any change in the energy to transition between the insulating and metallic phase.

ACKNOWLEDGMENTS

[1] T. M. Rice and D. McWhan, IBM J. Res. Dev. **14**, 251 (1970).

[2] L. Paolasini, C. Vettier, F. de Bergevin, F. Yakhou, D. Mannix, A. Stunault, W. Neubeck, M. Altarelli, M. Fabrizio, P. A. Metcalf, and J. M. Honig, Phys. Rev. Lett. **82**, 4719 (1999).

[3] J. C. Leiner, H. O. Jeschke, R. Valentí, S. Zhang, A. T. Savici, J. Y. Y. Lin, M. B. Stone, M. D. Lumsden, J. Hong, O. Delaire, W. Bao, and C. L. Broholm, Phys. Rev. X **9**, 011035 (2019).

[4] D. McWhan, A. Menth, J. Remeika, W. Brinkman, and T. M. Rice, Phys. Rev. B **7**, 1920 (1973).

[5] D. Wickramaratne, N. Bernstein, and I. I. Mazin, Phys. Rev. B **99**, 214103 (2019).

[6] J. G. Ramirez, T. Saerbeck, S. Wang, J. Trastoy, M. Malnou, J. Lesueur, J.-P. Crocombette, J. E. Villegas, and I. K. Schuller, Phys. Rev. B **91**, 205123 (2015).

[7] T. Saerbeck, J. de la Venta, S. Wang, J. G. Ramírez, M. Erekhinsky, I. Valmianski, and I. K. Schuller, J. Mater. Res. **29**, 2353 (2014).

[8] E. B. Thorsteinsson, S. Shayestehaminzadeh, and U. B. Arnalds, Appl. Phys. Lett. **112**, 161902 (2018).

[9] J. Brockman, M. Samant, K. Roche, and S. Parkin, Appl. Phys. Lett. **101**, 051606 (2012).

[10] Y. Kalcheim, N. Butakov, N. M. Vargas, M.-H. Lee, J. del Valle, J. Trastoy, P. Salev, J. Schuller, and I. K. Schuller, Phys. Rev. Lett. **122**, 057601 (2019).

[11] L. Dillemans, T. Smets, R. Lieten, M. Menghini, C.-Y. Su, and J.-P. Locquet, Appl. Phys. Lett. **104**, 071902 (2014).

[12] B. Allimi, S. Alpay, C. Xie, B. Wells, J. Budnick, and D. Pease, Appl. Phys. Lett. **92**, 202105 (2008).

[13] H. Schuler, S. Klimm, G. Weißmann, C. Renner, and S. Horn, Thin Solid Films **299**, 119 (1997).

[14] B. Sass, C. Tusche, W. Felsch, N. Quaas, A. Weismann, and M. Wenderoth, J. Phys. Condens. Matter **16**, 77 (2003).

[15] B. Allimi, M. Aindow, and S. Alpay, Appl. Phys. Lett. **93**, 112109 (2008).

[16] S. Yonezawa, Y. Muraoka, Y. Ueda, and Z. Hiroi, Solid State Commun. **129**, 245 (2004).

[17] P. Salev, J. del Valle, Y. Kalcheim, and I. K. Schuller, Proc. Natl. Acad. Sci. USA **116**, 8798 (2019).

[18] J. Sakai, M. Bavencoffe, B. Negulescu, P. Limelette, J. Wolfman, A. Tateyama, and H. Funakubo, J. Appl. Phys. **125**, 115102 (2019).

[19] F. Lechermann, N. Bernstein, I. I. Mazin, and R. Valentí, Phys. Rev. Lett. **121**, 106401 (2018).

[20] P. E. Blöchl, Phys. Rev. B **50**, 17953 (1994).

[21] G. Kresse and J. Hafner, Phys. Rev. B **47**, 558 (1993).

[22] G. Kresse and J. Furthmüller, Phys. Rev. B **54**, 11169 (1996).

[23] J. P. Perdew, K. Burke, and M. Ernzerhof, Phys. Rev. Lett. **77**, 3865 (1996).

[24] V. I. Anisimov, I. V. Solovyev, M. A. Korotin, M. T. Czyżyk, and G. A. Sawatzky, Phys. Rev. B **48**, 16929 (1993).

[25] P. Dernier and M. Marezio, Phys. Rev. B **2**, 3771 (1970).

[26] R. Moon, Phys. Rev. Lett. **25**, 527 (1970).